Konrad-Zuse-Zentrum
für Informationstechnik Berlin

Takustraße 7
D-14195 Berlin-Dahlem
Germany

R. GUL[1], CH. SCHÜTTE[1,2] AND S. BERNHARD [3]

[1]*Department of Mathematics and Computer Science, Freie Universität Berlin, Germany*

[2]*Zuse Institute Berlin, Germany*

[3]*Dept. of Electrical Engineering and Information Technology, Pforzheim University of Applied Sciences, Germany*

# Mathematical modeling and sensitivity analysis of arterial anastomosis in arm arteries

ZIB-Report 15–22 (April 2015)

Herausgegeben vom
Konrad-Zuse-Zentrum für Informationstechnik Berlin
Takustraße 7
D-14195 Berlin-Dahlem

Telefon: 030-84185-0
Telefax: 030-84185-125

e-mail: bibliothek@zib.de
URL: http://www.zib.de

ZIB-Report (Print) ISSN 1438-0064
ZIB-Report (Internet) ISSN 2192-7782

# Mathematical modeling and sensitivity analysis of arterial anastomosis in arm arteries

R. Gul[*], Ch. Schuette[†] and S. Bernhard[*‡]

**Abstract**

Cardiovascular diseases are one of the major problems in medicine today and the number of patients increases worldwide. To find the most efficient treatment, prior knowledge about function and dysfunction of the cardiovascular system is required and methods need to be developed that identify the disease in an early stage.

Mathematical modeling is a powerful tool for prediction and investigation of cardiovascular diseases. It has been shown that the Windkessel model, being based on an analogy between electrical circuits and fluid flow, is a simple but effective method to model the human cardiovascular system.

In this paper, we have applied parametric local sensitivity analysis (LSA) to a linear elastic model of the arm arteries, to find and rank sensitive parameters that may be helpful in clinical diagnosis. A computational model for end-to-side anastomosis (superior ulnar collateral anastomosis with posterior ulnar recurrent, SUC-PUR) is carried out to study the effects of some clinically relevant haemodynamic parameters like blood flow resistance and terminal resistance on pressure and flow at different locations of the arm artery. In this context, we also discuss the spatio-temporal dependency of local sensitivities.

The sensitivities with respect to cardiovascular parameters reveal the flow resistance and diameter of the vessels as most sensitive parameters. These parameters play a key role in diagnosis of severe stenosis and aneurysms. In contrast, wall thickness and elastic modulus are found to be less sensitive.
*Keywords: computational cardiovascular model, cardiovascular parameters, sensitivity analysis, anastomosis, Windkessel model.*
*AMS classification: 93B35, 70G60*

## 1 Introduction

With growing interest in the prediction and diagnosis of cardiovascular diseases, different mathematical models have been developed and applied. Windkessel models (electrical analogy to fluid flow) have shown to be an effective approach in modeling the human cardiovascular system [1–4, 6–9]. Westerhof, N. et al. [3] studied the

[*]Fachbereich Mathematik, Freie Universität Berlin, Germany. rgul@zedat.fu-berlin.de
[†]Fachbereich Mathematik, Freie Universität Berlin, and Zuse Institute Berlin, Germany. Christof.Schuette@fu-berlin.de
[‡]Dept. of Electrical Engineering and Information Technology, Pforzheim University of Applied Sciences, Germany. stefan.bernhard@hs-pforzheim.de

design, construction and evaluation of an electrical analog model. Quarteroni, A. et al. [1] introduced a multiscale approach, where local and systemic models are coupled at a mathematical and numerical level. He also introduced the Windkessel models for different inlet and outlet conditions.

Within the Windkessel model the hemodynamic state variables (pressure ($p$) and flow ($q$)), are interrelated to the model parameters like elastic modulus ($E$), vessel length ($l$) and its diameter ($d$), wall thickness ($h$), the density of blood ($\rho$) and the network structure. Provided that the model parameters applied characterize a certain cardiovascular disease, the Windkessel model is a good way to study variations of parameters, which are difficult to modify in reality. Thus the model parameters have a great impact on the result and validity of the simulations.

The basis for robust parameter estimation is on the one hand an optimal experimental measurement setup and on the other hand the development of models that describe the hemodynamic state variables in a set of relevant parameters that can be estimated with high accuracy. The design consists of several logical steps, dealing with questions like:

- Which vascular system parameters are most influential on the hemodynamic state variables pressure and flow?
- Which vascular system parameters are insignificant and may be fixed or eliminated?
- Which regions in flow and pressure waves are sensitive w.r.t. cardiovascular parameters?
- How meaningful are the clinically relevant cardiovascular parameters in arterial anastomosis?

Sensitivity analysis is a powerful approach to find sensitive and therefore important cardiovascular system parameters [10–13]. The sensitive parameters can be further used to design a measurement setup and to interpret measurements. In [14] for example, Sato, T. et al. studied the effects of compliance, volume and resistance on cardiac output using sensitivity analysis. Yih-Choung Yu et al. [15] used parameter sensitivity to construct a simple cardiovascular model. Leguy, C.A.D et al. [20] applied global sensitivity analysis on the arm arteries and showed that the elastic modulus is most sensitive parameter, while arterial length is a less sensitive parameter.

## 1.1 Scope of the current work

In this paper, we are interested how structural changes, like for example anastomosis influence local sensitivities. Anastomoses are the interconnection between vessels, which provide a collateral circulation and also act as a second rout of blood flow when main vessels are blocked by plaque, atherosclerosis or stenosis, to minimize the damages at tissue level.

Another important concept found in the context of anastomosis is valve-less flow. William Harvey published a report explaining "impedance defined flow", which explained a mechanism for valve-less flow [16]. Later on, Weber [17] stated that the heart is not able to pump blood alone, but there are other forces which help

in circulation. There are several structural aspects in the cardiovascular system, which control the blood flow or simply create valve-less flow like, viscous and inertial effects and also elastic properties of two vessels [18]. Details of the valve-less flow mechanism are given in [19] and will not be discussed here in detail. Further, we will not discuss turbulent effects that appear in merging flows at the end-to-side anastomosis, which mainly depend upon the angle and flow rate of the merging vessels.

In this paper, we present a computational model of anastomosis around the elbow joint (SUC-PUR), using the lumped parameter approach. As luminal diameter or equivalently the flow resistance is the most important parameter in blood flow through anastomosis, we study the effects of viscous flow resistance and terminal impedance on pressure and flow through anastomosis.

In a first instance, we apply local sensitivity analysis (without anastomosis) to study the effects of cardiovascular parameters on the hemodynamic state variables. We study time dependent sensitivities w.r.t. flow resistance, distensibility and inertial forces to find sensitive regions in the pressure and flow waves. Due to the network structure of the cardiovascular system it is helpful to determine and discuss the location dependent sensitivities, i.e. which locations in the arm arteries are sensitive to which parameters. Further, in arterial anastomosis, we also discuss the effects of flow control parameters, flow resistance and terminal resistance on cardiovascular pressure and flow at selected nodes. Finally, to quantify and compare the results, we apply the concept of norms.

With this work, we intend to validate different methodologies of local sensitivity analysis, using a simple example problem of the arm artery to show the principle agreement with Ohm's law of hydrodynamics. The method may then be used to analyze more complex cardiovascular network structures in the future.

## 2 Derivation of the model equations

Under the assumption that the arterial tree is decomposed into short arterial segments of length $l$ with a constant circular cross-section and linear elastic wall behavior, the following one dimensional flow equations can be derived from the linearized Navier-Stokes equation, the equation of continuity and the shell-equation for thin walled, linear elastic tubes [1, 21]

$$-\frac{\partial p}{\partial x} = \mathcal{R}q + \mathcal{L}\frac{\partial q}{\partial t}, \tag{1}$$

$$-\frac{\partial q}{\partial x} = \frac{p}{\mathcal{Z}} + \mathcal{C}\frac{\partial p}{\partial t}. \tag{2}$$

Within these equations, the state variables are the flow, $q$ and the transmural pressure, $p$. The viscosity and inertial forces of blood flow are described by the viscous flow resistance, $\mathcal{R}$ and blood inertia, $\mathcal{L}$ per unit length respectively. The elastic properties of the wall are modeled by a compliance, $\mathcal{C}$ per unit length, while $\mathcal{Z}$ is the terminal impedance [21].

Integration of the two partial differential eqns. (1) and (2) along the flow axis, leads to a system of equations (3) commonly used to describe electrical circuits of the form given in figure 1. In this type of model each segment of the arterial system

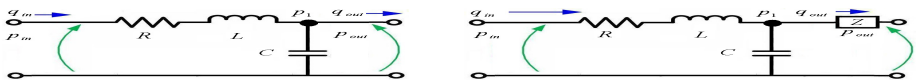

Figure 1: Linear elastic model for fluid flow in non-terminal vessel segments (left) and for terminal vessel segments (right).

is described by a set of two equations that are known as Windkessel equations. Here $(p_{in}, q_{out})$ and $(p_{in}, p_{out})$ are the boundary conditions for non-terminal and terminal nodes respectively. In this study, pressure is used as an input boundary condition (see figure 2) and to model a mean venous pressure with a value of 15mmHg for terminal nodes, the equation system is setup by including an additional terminal node with terminal impedance, $Z$ (see figure 1, (right) and eqn. 4). The matrix form of the Windkessel eqns. with boundary conditions is

$$\frac{d\mathcal{X}}{dt} = A\mathcal{X} + B, \tag{3}$$

where $\mathcal{X} = \{q_1, p_1, ..., q_{N_s}, p_{N_s}\}$ is the state vector, $A$ is the state matrix and $B$ contains the boundary conditions.
***For non-terminal segments*** (figure 1, left) $\mathcal{X} = (q_{in}, p_{out})^T$

$$A = \begin{pmatrix} \frac{-R}{L} & \frac{-1}{L} \\ \frac{1}{C} & 0 \end{pmatrix}, \qquad B(p_{in}, q_{out}) = \begin{pmatrix} \frac{p_{in}}{L} \\ -\frac{q_{out}}{C} \end{pmatrix}$$

***For terminal segments*** (figure 1, right) $\mathcal{X} = (q_{in}, q_{out})^T$

$$A = \begin{pmatrix} \frac{-R}{L} & \frac{-1}{L} \\ \frac{1}{C} & -\frac{1}{ZC} \end{pmatrix}, \qquad B(p_{in}, p_{out}) = \begin{pmatrix} \frac{p_{in}}{L} \\ -\frac{p_{out}}{ZC} \end{pmatrix}$$

A complete description of the state-space representation of a network structure is given in section 2.3. The electrical parameters for $i$-th non-terminal and $j$-th terminal segment are defined as,

$$R_i = \frac{8\nu l_i}{\pi r_i^4}, \qquad L_i = \frac{\rho l_i}{\pi r_i^2}, \qquad C_i = \frac{2\pi r_i^2 l_i}{E_i h_i}, \qquad Z_j = \frac{p_j - p_{out}}{q_{out}} \tag{4}$$

where

$E$ – Young modulus, $l$ – length of vessel, $r$ – radius of vessel
$h$ – wall thickness, $\nu$ – blood viscosity, $\rho$ – blood density

The vascular network parameters, to setup matrices $A$ and $B$ are given in Table 1.

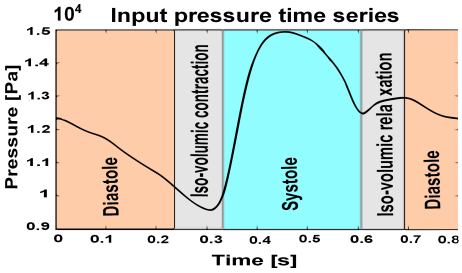


Figure 2: The input pressure time series and cardiac phases, which are used as an input boundary condition.

| Nodes | $E$ | $l$ | $d$ | $h$ | $R$ | $C$ | $L$ |
|---|---|---|---|---|---|---|---|
| *units* | $kgm^{-2}s^{-2}$ $*10^5$ | $m$ $*10^{-2}$ | $m$ $*10^{-3}$ | $m$ $*10^{-4}$ | $kgs^{-1}m^{-4}$ $*10^6$ | $m^4s^2kg^{-1}$ $*10^{-11}$ | $kgm^{-4}$ $*10^6$ |
| 1 | 4 | 6.1 | 7.28 | 6.2 | 3.539 | 7.454 | 1.539 |
| 2 | 4 | 5.6 | 6.28 | 5.7 | 5.868 | 4.778 | 1.898 |
| 3 | 4 | 6.3 | 5.64 | 5.5 | 10.15 | 4.035 | 2.648 |
| 4 | 4 | 6.3 | 5.32 | 5.3 | 12.82 | 3.514 | 2.976 |
| 5 | 4 | 6.3 | 5 | 5.2 | 16.43 | 2.974 | 3.369 |
| 6 | 4 | 4.6 | 4.72 | 5 | 15.10 | 1.9 | 2.76 |
| 7 | 8 | 7.1 | 3.48 | 4.4 | 78.90 | 0.667 | 7.838 |
| 8 | 8 | 7.1 | 3.24 | 4.3 | 105 | 0.531 | 9.042 |
| 9 | 8 | 7.1 | 3 | 4.2 | 142.9 | 0.448 | 10.55 |
| 10 | 8 | 2.2 | 2.84 | 4.1 | 55.11 | 0.1207 | 3.647 |
| 11 | 8 | 6.7 | 4.3 | 4.9 | 31.94 | 1.067 | 4.844 |
| 12 | 16 | 7.9 | 1.82 | 2.8 | 1173 | 0.0834 | 31.88 |
| 13 | 8 | 6.7 | 4.06 | 4.7 | 40.19 | 0.9366 | 5.434 |
| 14 | 8 | 6.7 | 3.48 | 4.6 | 50.22 | 0.80 | 6.075 |
| 15 | 8 | 3.7 | 3.66 | 4.5 | 33.60 | 0.3958 | 3.693 |
| 16 | 8 | 6 | 2.3 | 1.95 | 349 | 0.366 | 15.16 |
| 17 | 8 | 6 | 2 | 1.7 | 611 | 0.277 | 20 |
| 18 | 16 | 6 | 1.8 | 1.53 | 931 | 0.112 | 24.75 |

Table 1: Numerical values of parameters for each node of the arm arteries (shown in figure 4). The value of terminal resistance ($Z$) on three terminal nodes is $3.24 * 10^9$ $kgs^{-1}m^{-4}$, $\nu = 0.004$ $kgs^{-1}m^{-1}$ and $\rho = 1050$ $kgm^{-3}$ [4, 5].

## 2.1 Network structure and model equations

To generate the model of the arm arteries (with and without anastomosis), we use domain decomposition (DD) approach, in which the whole cardiovascular system is decomposed into a number of vascular segments, where the parameters are approximately constant. Each segment of the arm arteries in a network structure as given in figure 4, is represented by an electrical circuit as shown in figure 1.
Decomposition into vascular segments, however, requires relations between the arterial segments to reconstruct the network structure of the arterial tree. Therefore

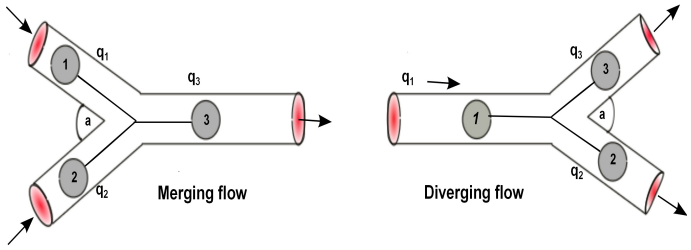


Figure 3: Model geometry for merging and diverging flows at junctions.

we define bifurcation conditions for the mother and daughter vessels as follows:

$$q_1 = q_2 + q_3, \quad \text{(diverging)} \tag{5}$$
$$q_3 = q_1 + q_2, \quad \text{(merging)} \tag{6}$$
$$p_1 = p_2 = p_3 \tag{7}$$

These conditions are derived from conservation of mass and momentum, i.e. pressure is constant and flow has to be conserved at the bifurcation (see figure 3). For more details see [9].

### 2.1.1 Model equations without anastomosis

In analogy to Kirchhoff's current and voltage law (Ohm's law of hydrodynamics), the arterial structure given in figure 4, leads to the following system of coupled ordinary differential equations for pressure and flow:
*Flow equations:*

$$\begin{aligned} \dot{q}_i &= \frac{p_{i-1} - p_i - R_i q_i}{L_i}, \; i = 1, 2, ..., 15, \text{and } i \neq 11 \\ \dot{q}_{11} &= \frac{p_6 - p_{11} - R_{11} q_{11}}{L_{11}} \end{aligned} \tag{8}$$

*Pressure equations:*

$$\begin{aligned} \dot{p}_i &= \frac{q_i - q_{i+1}}{C_i}, \quad i = 1, ..., 15 \text{ and } i \neq 6, 10, 11, 12, 15 \\ \dot{p}_6 &= \frac{q_6 - q_{11} - q_7}{C_6}, \quad \dot{p}_{11} = \frac{q_{11} - q_{12} - q_{13}}{C_{11}} \quad \text{(at bifurcation)} \\ \dot{p}_{2i+8} &= \frac{q_{2i+8} - (p_{2i+8} - p_{out})/Z_i}{C_{2i+8}}, \quad i = 1, 2, 3 \quad \text{(at terminals)} \end{aligned} \tag{9}$$

### 2.1.2 Model equations with anastomosis

From the network structure of the arm artery with SUC-PUR anastomosis (see figure 4), it is evident, that the flow will split at nodes 3 and 6, and will merge at node 11. Further the inlet pressure at node 11 is the same as in nodes 6 and 18. The additional equations for three nodes of SUC-PUR anastomosis are,

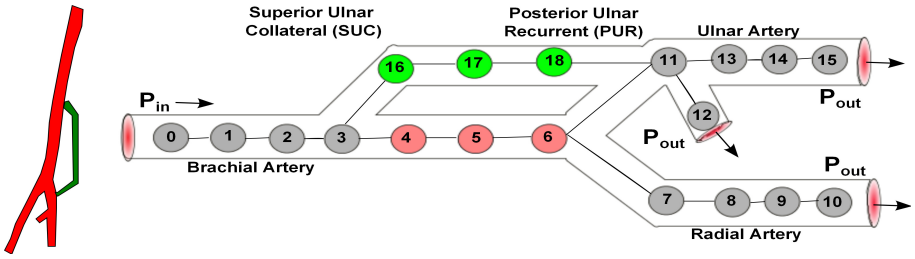


Figure 4: Simplified anatomy of the arm arteries (left) and model geometry of brachial, superior ulnar collateral anastomosis with posterior ulnar recurrent (SUC-PUR), ulnar and radial arteries (right). The number of segments is $N_s = 15$ (without anastomosis) and $N_{as} = 18$ (with anastomosis), both with $N_t = 3$ terminal nodes.

*Anastomosis flow equations:*

$$\dot{q}_{16} = \frac{p_3 - p_{16} - R_{16}q_{16}}{L_{16}} \quad \dot{q}_{17} = \frac{p_{16} - p_{17} - R_{17}q_{17}}{L_{17}} \quad \dot{q}_{18} = \frac{p_{17} - p_6 - R_{18}q_{18}}{L_{18}} \tag{10}$$

*Anastomosis pressure equations:*

$$\dot{p}_3 = \frac{q_3 - q_4 - q_{16}}{C_3}, \quad \dot{p}_{16} = \frac{q_{16} - q_{17}}{C_{16}}, \quad \dot{p}_{17} = \frac{q_{17} - q_{18}}{C_{17}}, \quad \dot{p}_{18} = \frac{q_{18} + q_6 - q_{11}}{C_6 + C_{18}} \tag{11}$$

According to the conservation of momentum the pressure at nodes 18 and 6 is identical.

## 2.2 Diverging and merging flows at junctions

Blood flow at junctions plays an important role in normal and pathological conditions of the cardiovascular system. In this section, we briefly discuss pressure and flow at junctions for both diverging (at bifurcations) and merging blood flows. In the arterial system, merging flow conditions appear in the context of anastomosis.

### 2.2.1 Diverging blood flow

In the arm artery structure, given in figure 4, diverging flows occur at the bifurcation of the vessels at nodes 3, 6 and 11. The mass conservation equation for linearized system (eqns. 12, 13) at node 3 is, $q_3 = q_{16} + q_4$ and the total pressure is constant at the bifurcation, i.e. the output pressure at node 3 is the input pressure for both nodes 16 and 4. In this paper, we limit our study to symmetric and asymmetric bifurcations with respect to the radius of the daughter vessels.

### 2.2.2 Merging blood flow

To model the merging flows at junctions has a great importance to understand the effect of anastomosis and bypass in the cardiovascular system. These type of flows occur also in vascular grafting and arteriovenous fistula (AVF). According to the

conservation of mass, the flow at node 11 is, $q_{18} + q_6 = q_{11}$ and according to the law of conservation of momentum, the total pressure remains continuous at node 11.

## 2.3 State-space representation

The state-space representation is a compact way to model a physical system as a set of input, output and state variables related by first order differential equations [22]. In state-space form, we have a system of two equations: an equation for determining state $x_t$ of the system (state equation), and another equation to describe the output $y_t$ of the system (observation equation). The matrix form can be written as

$$\dot{x}_t = Ax_t + Bu_t, \tag{12}$$
$$y_t = Cx_t + Du_t. \tag{13}$$

Here, $x_t$, is the state vector of the system, $u_t$ the input vector and $y_t$, the observation vector. The dynamics of the system is described by the state dynamics matrix, $A \in M(n \times n)$. The input matrix, $B \in M(n \times i)$ specifies the time dependency on boundary conditions (BC) applied at in- and outflow locations and the observation matrix, $C \in M(m \times n)$ defines the observation locations within the state-space system, i.e. the nodal location in the network. Here, $m$ denotes the number of observations. Finally, the input to observation matrix, $D \in M(m \times i)$ models the influence of the input vectors and accounts for the observation of the BC. Besides its computational advantage, the state-space form allows for the integration of experimental measurements (observations) into the model building process. This step is essential for the adjacent model parameter estimation from experimental measurements, that are planned in a future study.

The state vector, $x_t$, contains the flow and pressure functions at all network locations, whereas, the output vector, $y_t$ contains the flow and pressure at selected nodes $i$. For a $m = 4$ dimensional observation vector, the output vector is $y(t) = (q_5(t), p_5(t), q_6(t), p_6(t))^T$, where $y \in R^m$ at nodes 5 and 6. The state-space system for the arm artery given in figure 4, using eqn. (8) and eqn. (9) is defined by

$$A_{ij} = \begin{cases} \frac{-R_{\frac{i+1}{2}}}{L_{\frac{i+1}{2}}} & i = 1, 3, 5, ...29, j = i \\ \frac{1}{C_{\frac{i}{2}}} & i = 2, 4, 6, ...30, j = i - 1 \\ \frac{-1}{L_{\frac{i+1}{2}}} & i = 1, 3, 5, ...29, j = i + 1 \\ \frac{1}{L_{\frac{i+1}{2}}} & i = 3, 5, 7, ...29, j = i - 1 \quad \text{and} \quad i \neq 21, 25 \\ & \text{also for} \quad i = 21, j = 12 \quad \text{and} \quad i = 25, j = 22 \\ \frac{-1}{C_{\frac{i}{2}}} & i = 2, 4, 6, ...30, j = i + 1 \quad \text{and} \quad i \neq 20, 24 \\ & \text{also for} \quad i = 12, j = 21 \quad \text{and} \quad i = 22, j = 25 \\ \frac{-1}{Z_k C_{\frac{i}{2}}} & k = 1, 2, 3, \quad i = 20, 24, 30, \quad j = i \\ 0 & \text{otherwise} \end{cases}$$

$$B_{ij} = \begin{cases} \frac{1}{L_i} & i = j = 1 \\ \frac{1}{Z_{j-1} C_{\frac{i}{2}}} & i = 20, j = 2 \\ \frac{1}{Z_{j-1} C_{\frac{i}{2}}} & i = 24, j = 3 \\ \frac{1}{Z_{j-1} C_{\frac{i}{2}}} & i = 30, j = 4 \\ 0 & \text{otherwise} \end{cases}, \; C_{ij} = \begin{cases} 1 & i = 1, 2, 3, 4, j = i + 8 \\ 0 & \text{otherwise} \end{cases}$$

and $D_{ij} = 0$. The system with SUC-PUR anastomosis, we expand our state-space model by using eqns. (10, 11). The system is solved using MATLAB built in solvers 'ode45' and 'lsim'.

# 3 Methods of local sensitivity analysis

To understand how the cardiovascular model parameters influence the state variables, we perform sensitivity analysis. Mathematically the sensitivity coefficient can be calculated as

$$S_{ij} = \frac{\partial y_i}{\partial \theta_j}, \tag{14}$$

where $y_i$ is the $i$-th model output and $\theta_j$ is the $j$-th model parameter.

The sensitivity coefficients $S_{ij}$ can also be computed by means of the *direct differential method* (DDM), which solves the system of differential equations for sensitivity coefficients (for complete derivation, see Appendix $\mathbb{A}$)

$$\dot{S} = f_\theta + J \times S. \tag{15}$$

The sensitivity coefficients matrix $S = (S_{ij})$ can be obtained by solving model equations (12, 13) simultaneously with the system (eqn. 15) using an appropriate ODE solvers. A drawback associated with DDM is that the Jacobian needs to be computed which is time consuming for large-scale problems [23].

## 3.1 Sensitivity by finite difference method

In local sensitivity analysis, parameters are varied segmentwise by some portion around a fixed value (nominal value) and the effects of individual perturbations on the observations are studied [23]. Using differential calculus the sensitivity coefficients are

$$S_i = \frac{\partial y_i}{\partial \theta} = \lim_{\Delta\theta \to 0} \frac{y_i(\theta + \Delta\theta) - y_i(\theta)}{\Delta\theta}, \tag{16}$$

where, $y_i$ is the $i$-th model output, $\theta$ is the set of model input parameters and $\Delta\theta$ is the change in model parameters. There are various methods to compute the sensitivity coefficients in eqn. (16). Within this work, we use a first order *finite difference* for approximation

$$S_i = \frac{\partial y_i}{\partial \theta} \simeq \frac{y_i(\theta + \Delta\theta) - y_i(\theta)}{\Delta\theta}. \tag{17}$$

Eqn. (17) produces a set of two sensitivity time series, $S_i(t)$ (one for pressure and one for flow) per parameter and per network node (see figure 8).

### 3.2 Sensitivities by using norms

Another method to quantify changes to the state variables due to a change in model parameters is to introduce a norm. To obtain a measure that validates the sensitivities, we compute the mean Euclidean distances of the observations made in a model with different parameter sets $\theta_1$, $\theta_2$. Here $\theta_1$ is the nominal parameter set and $\theta_2$ is a parameter set with $\pm 10\%$ change in $\theta_1$.

$$\|\theta_1, \theta_2\| := \underset{t \in T}{mean} \frac{\| \ y_i(\theta_2, t) - y_i(\theta_1, t) \ \|_2}{\|y_i(\theta_1, t)\|_2} \qquad i = 1, 2, 3...2 \times N_s,$$

## 4 Results and discussion

In this section, we discuss different scenarios for sensitivity analysis like, e.g. sensitivity with respect to structural parameters, $Eldh$, electrical parameters, $RCL$ (without anastomosis), time and network location dependent sensitivities and impact of blood flow resistance, R and terminal resistance, Z on state variables (with anastomosis). The sensitivity results are finally compared to the 2-norm of the distance vector of the state variables of two time series.

### 4.1 Sensitivities with respect to E, l, d and h

To study the effects of $Eldh$ on pressure and flow, we first solve our model with both $\pm 10\%$ variation of $Eldh$ from its nominal values (see table 1). The sensitivities are computed using eqn. (17) by setting $\theta$ either to $E, l, d$ or $h$. The sensitivities for pressure and flow w.r.t $Eldh$ were calculated at node 7 (radial artery) and plotted in figure 5.

From eqn. 4, elastic modulus, $E$ is inversely proportional to the compliance of the vessel, i.e. variation in elastic modulus changes the compliance of vessel, which causes phase and amplitude shift of the pressure and flow waves, as a result the pulse transit time (PTT) changes because pressure and flow wave speed is influenced. E and h appear as factor pair in eqn. 4, thus their sensitivity is common and not separable (see figure 5, $A_1, A_2, A_7, A_8$).

Phase and amplitude shift while changing $l$ is due to the dependence of $R, C$ and $L$ on vessel length (eqn. 4), also due to the longer and shorter travel time of pressure and flow waves (see 5, $A_3, A_4$). Vessel length is most sensitive at early systole, end systole and end diastole.

As diameter is directly proportional to blood flow rate, which means increasing the diameter of the vessel will increase the flow and pressure and vice versa. From figure 5 ($A_5, A_6$), it is clearly evident, that the diameter is most sensitive at the peak systole and end systole.

### 4.2 Sensitivities with respect to R, C and L

The sensitivity of the electrical parameters $R, C$ and $L$ on cardiovascular pressure and flow are found by solving eqns. (12) and (13) numerically using the CVODES solver, which is a part of SUNDIALS software suit [24, 25] and then calculate the sensitivities using eqn. (17). The sensitivity patterns in figure 7 where obtained by variation of $R, C$ and $L$ in the arm arteries (with and without anastomosis). The

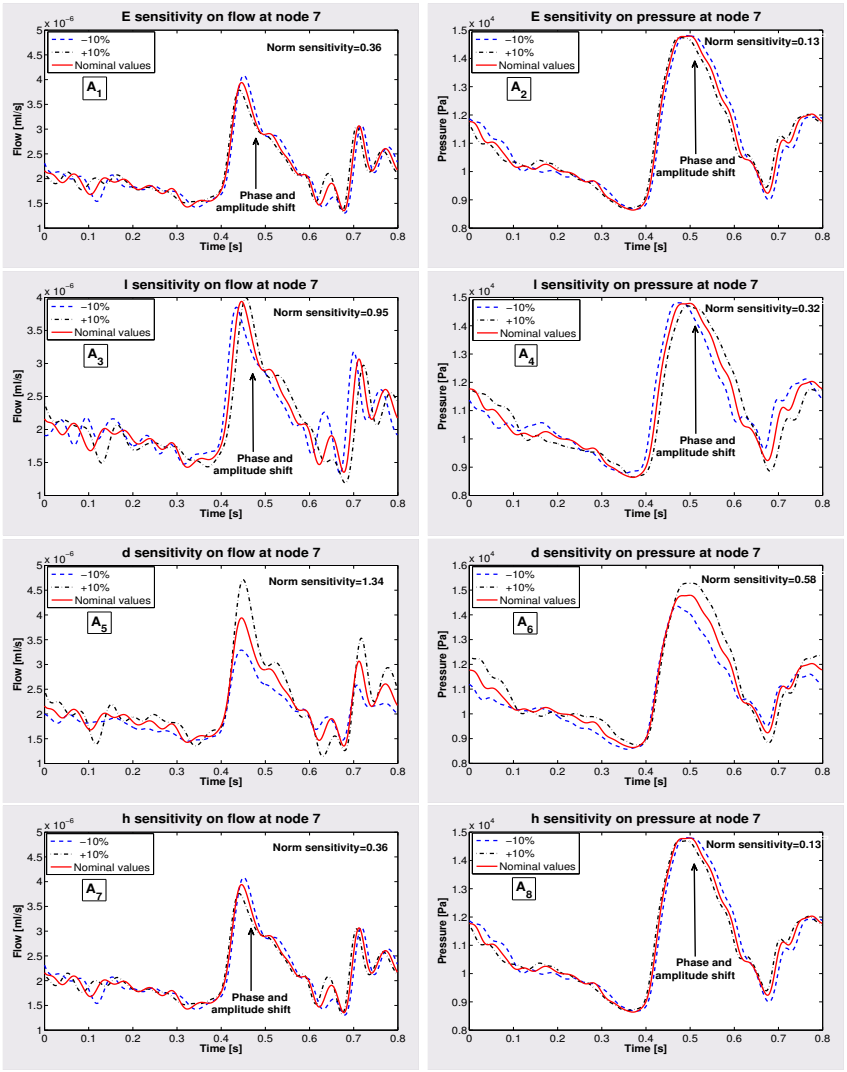


Figure 5: Pressure and flow for a ±10% change in $E$, $l$, $d$ and $h$ in the radial artery at node 7. The results reveal that $d$ and $l$ are sensitive parameters, while $E$ and $h$ are less sensitive. Due to the linear appearance of $E$ and $h$, the effect on cardiovascular pressure and flow is identical.

matrix diagonal displays the local sensitivities within the segments of variation itself and the off diagonals are related to the sensitivities of upstream and downstream segments (figure 6).

The sensitivities of viscous flow resistance, $R$ on flow in brachial artery indicate only a local effect at inlet and a small downstream effect on radial and ulnar arteries, while there is no upstream effect (see figure 7, $C_1$). For pressure, changing $R$ in brachial artery has local effect with strong downstream sensitivity on radial and ulnar while negligible effect was found from radial to ulnar and from ulnar, radial

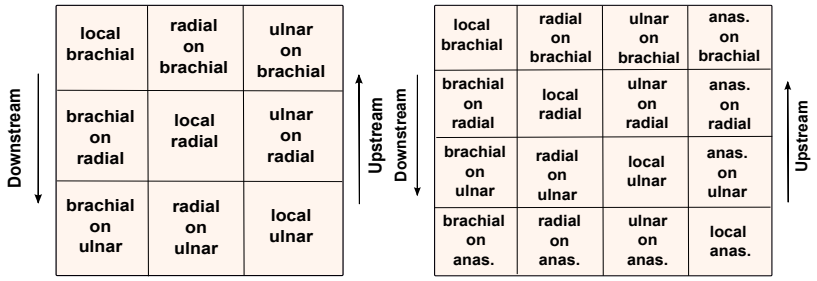


Figure 6: Sensitivity pattern in arm artery without anastomosis (left) and with anastomosis (right), obtained by changing the values of cardiovascular parameter $R, C$ and $L$.

to brachial. Results show strong reflections from the terminal nodes, 10 12 and 15 (see figure 7, $C_2$).

Further, the flow resistance, $R$ in the parallel association of the ulnar and radial arteries has negligible downstream and upstream sensitivities, because in parallel arteries the total flow resistance is given by the fraction $\frac{1}{R_{total}} = \frac{1}{R_{ulnar}} + \frac{1}{R_{radial}}$, i.e. due to the increment in total diameter, the over all flow resistance reduces. Physically a change of $R$ in one branch redirects the flow into the other branch while the overall flow is maintained. The sensitivity of flow resistance in parallel branches is thus smaller than in series connections.

The results indicate that the arterial compliance, $C$ has small downstream influence on the flow for all segments of the arm artery and strong upstream global sensitivity from radial to brachial and ulnar to brachial. This effect is evidently caused by wave reflections at the terminal nodes, 10, 12 and 15 of the radial and ulnar artery respectively. In contrast, for the pressure, only local effects are observed in terminal branches (see figure 7, $C_3, C_4$).

From eqn. (4), it is obvious, that the viscous resistance and the blood inertia are inversely related to $r^4$ and $r^2$ respectively. Which means in large arteries blood inertia plays an important role, while in small arteries viscous resistance is more important. A variation of blood inertia in the inlet node of the brachial artery has large local influence on flow, while for pressure, changing $L$ in brachial artery has downstream influence on all following nodes and upstream influence was observed from the terminal nodes of the radial and ulnar artery due to reflections (see figure 7, $C_5, C_6$). Furthermore, due to the fact that the total inductance $\frac{1}{L_{total}} = \frac{1}{L_{ulnar}} + \frac{1}{L_{radial}}$ reduces at the bifurcation, the flow and pressure in the ulnar and radial arteries are less sensitive with respect to $L$.

## 4.3 Time dependent sensitivity

For time dependent sensitivity, we first solve eqns. (12) and (13) with Matlab built in solvers, then calculate sensitivity time series for both pressure and flow at nodes 5 and 7 by using eqn. (17). The results of time dependent sensitivity analysis contain several aspects that are important especially in the estimation of cardiovascular parameters from pressure and flow waves. It is well known, that parameters that are sensitive for pressure and flow can be estimated with high accuracy, while insensitive

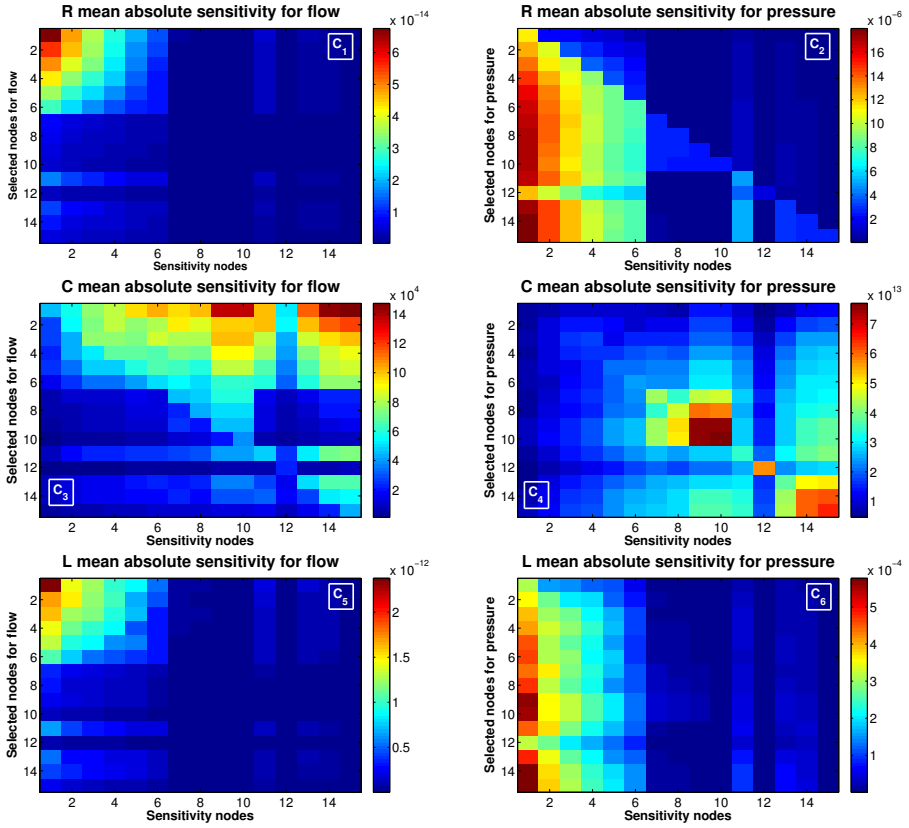


Figure 7: Effects of viscous flow resistance $R$ (top), vessel compliance $C$ (middle) and blood inertia $L$ (bottom) on pressure and flow in the arm arteries. Changes in the flow resistance, $R$, and blood inertia, $L$, in brachial artery have strong local effects on flow and have significant downstream effects on radial and ulnar pressure.

parameters cannot be estimated at all. Thus the identification of sensitive regions with the cardiac cycle could benefit parameter estimation. In other words, if only sensitive regions of the flow and pressure waves are used then a better estimation of parameters is expected.

In this section, we study +10% change in $R$, $C$ and $L$ in all locations. Pressure and flow sensitivity time series w.r.t $R$, $C$ and $L$ were calculated at node 7 (see figure 8) by using eqn. (17). The results are summarized as follows:

*(a) R sensitivity time series:* According to the hydrodynamic form of Ohm's law, the flow resistance, $R$ can be calculated from the ratio of pressure gradient and flow, i.e. $R = \frac{\Delta p}{q}$. It is clear from figure 8 $(B_1, B_2)$ that flow resistance has an inverse relationship to blood flow, $q$ and has linear relationship with the transmural pressure, $p$. Due to the fact, the resistance increases for constricting arteries and decreases for dilating arteries, the flow resistance is most sensitive in end systole, early and end diastole of the flow wave, while it is less sensitive in the early systole. On the other hand, sensitivity of flow resistance is proportional to the pressure and

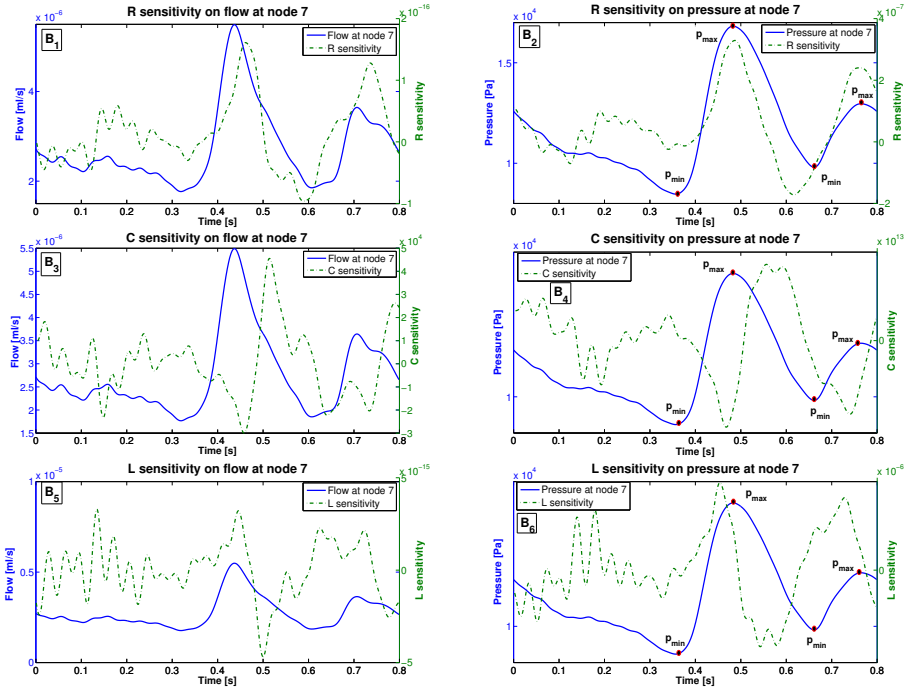


Figure 8: Sensitivity time series for both pressure and flow waves at node 7, with respect to $R$ $(B_1, B_2)$, $C$ $(B_3, B_4)$ and $L$ $(B_5, B_6)$. Results show that the flow is sensitive to variations of $R$ at the end of systole and end of diastole, while the pressure is sensitive in early systole and early diastole. In contrast the pressure is sensitive to $C$ in end systole and end diastole and to $L$ in early systole and early diastole.

significant sensitivities were found in early systole, early diastole and at $p_{max}$, while flow resistance has less sensitivity at $p_{min}$, which shows a clear agreement with Ohm's law of hydrodynamics.

*(b) C sensitivity time series:* Compliance, $C$ is the change in arterial blood volume $dV$, due to the change in arterial blood pressure $dp$, i.e. $C = \frac{dV}{dp}$. It is thus the slope of the pressure-volume curve, so it depends on the pressure level at which the compliance or elastance is calculated. The results reveal, the compliance has a larger effect on systole and diastolic of the flow wave. For pressure, C is most sensitive at end systole, end diastole and $p_{max}$. Low sensitivity was found at $p_{min}$ (see figure 8 $(B_3, B_4)$).

*(c) L sensitivity time series:* Blood inertia, $L$ relates pressure drop with flow rate i.e. $L = \frac{\Delta p}{\dot{q}}$. Blood inertia plays a role in acceleration (in systole) and deceleration (in diastole) of the blood flow in the vessels. Figure 8 $(B_5, B_6)$ clearly shows, that $L$ sensitivity time series has inverse relationship to the pressure and flow waves. Blood inertia is sensitive at systole and diastole of the flow wave while peak sensitivity was found for the pressure at early systole, early diastole and at

end diastole. Furthermore, pressure is insensitive at $p_{max}$ and $p_{min}$.

## 4.4 Network location dependent sensitivities

In order to identify important locations in arm arteries (without anastomosis), we assume a non physiological network structure with identical node parameterization, i.e. the parameters Ri, Ci and Li are identical to node 1. This leads to equally weighted sensitivities in the network, thus the sensitivity is only influenced by location and network structure of the arm artery.

Results show, $R$ is sensitive for flow in brachial artery with small downstream sensitivity on radial and ulnar arteries and almost no upstream sensitivity from radial and ulnar to brachial artery (see figure 9, $D_1$). On the other hand, changes of $R$ in brachial artery have local and strong downstream influence on pressure for all following nodes of radial and ulnar arteries. However, no upstream sensitivities were found from radial and ulnar to brachial artery. For pressure, results also show the sensitivities from terminal segments, 10, 12 and 15 back to brachial artery due to reflections (see figure 9, $D_2$). In figure 9 ($D_3, D_4, D_5, D_6$), the sensitivity results of $C$ and $L$ are scattered, which reveal that the effect of $C$ and $L$ can only be seen if a physiological network structure like in figure 7 is taken.

## 4.5 Sensitivity with anastomosis

Blood flow in SUC-PUR anastomosis (collateral circulation) depends on the size and mainly on the diameter of the anastomosis, smaller diameters reduce the flow in anastomosis and vice versa. In this paper, we focus the study on end-to-side anastomosis and show the sensitivity of the anastomosis structure on pressure and flow by changing flow resistance, $R$ and terminal impedance, $Z$. Moreover, we discuss four different scenarios of arterial anastomosis sensitivity, which are

*(a) R sensitivity when,* $\{RCL\}_a \simeq \{RCL\}_b$*:* In order to study the influence of flow resistance through arterial anastomosis, identical values of $RCL$ are taken for both anastomosis and its parallel brachial artery, i.e. $\{RCL\}_a \simeq \{RCL\}_b$. Here $\{RCL\}_a$ are parameter values of anastomosis nodes (16, 17 and 18) and $\{RCL\}_b$ are parameter values of brachial nodes which appear in parallel to anastomosis nodes (4, 5 and 6) and the equality means that corresponding anastomosis nodes have identical parameter values, segmentwise as its counterpart brachial nodes.

As it is mentioned earlier, the diameter or equivalently the blood resistance plays an important role in pressure and flow distribution of cardiovascular system, so we limit our study in changing the blood resistance in the arterial anastomosis. For flow, $R$ is sensitive locally at nodes 1,2, and 3 specially most sensitive at inlet. Due to identical network parameters, the downstream sensitivity from first three nodes of brachial artery on anastomosis and its parallel brachial artery is the same. More importantly, changing $R$ in anastomosis or its counter part brachial artery has the same local and upstream/downstream influence on each other (see figure 10, $E_1$). For pressure, $R$ is sensitive at first three nodes and has strong downstream sensitivities on all following segments and upstream sensitivities can be seen from the terminal nodes because of reflections (see figure 10, $E_2$).

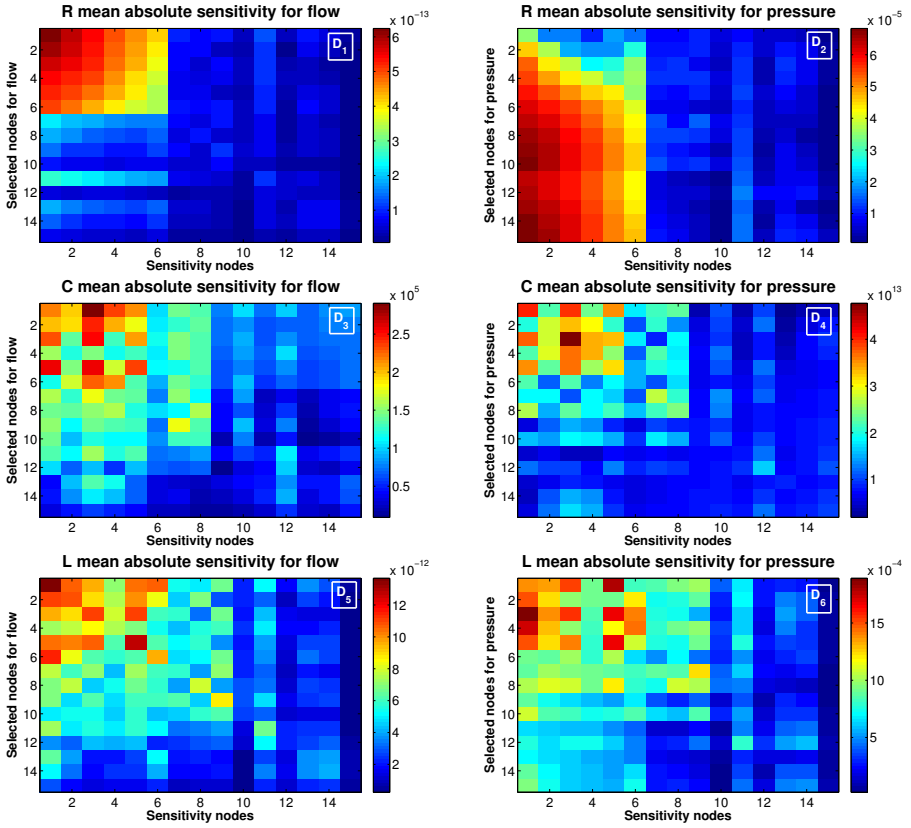


Figure 9: Effects of viscous flow resistance $R$ ($D_1, D_2$), vessel compliance $C$ ($D_3, D_4$) and blood inertia $L$ ($D_5, D_6$) on pressure and flow in the arm artery (with identical node values). From the results $R$ is a sensitive parameter for local flow in brachial artery and has both local (in brachial) and global downstream effect on pressure.

*(b) R sensitivity for ideal case:* A physiological network with an arterial anastomosis is taken, based on parameter values given in table 1. From eqn. 4, it is clear that a decrease in diameter or equivalently increase in total blood resistance of anastomosis decreases the mean flow. For flow, $R$ is locally sensitive at first three nodes and has significant downstream influence on brachial artery particularly on the anastomosis. The former sensitivity is because of backflow caused by pressure drop resulting from the increased blood resistance of the anastomosis (see figure 10, $E_3$). For pressure, $R$ is sensitive locally at first three nodes and has strong downstream sensitivity on radial, ulnar and SUC-PUR anastomosis (see figure 10, $E_4$).

*(c) R sensitivity of ideal case with large Z:* When a body has no physical activity then the terminal resistance (impedance) has a large value (here, $Z_L = 30Z$). By increasing $Z$, flow will reduce and pressure increase near the terminals. For flow, $R$ is sensitive at nodes 1, 2 and 3 with strong downstream sensitivities on the

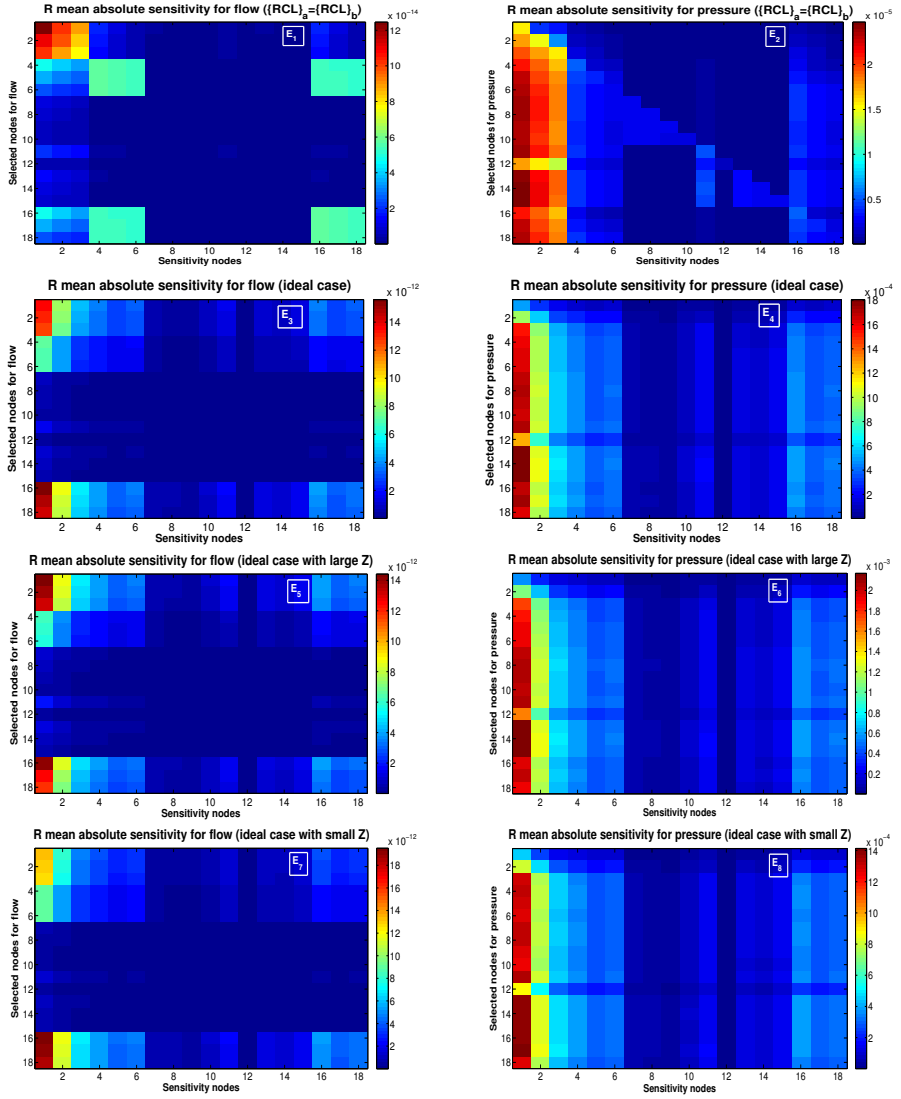


Figure 10: Effects of viscous flow resistance $R$ and terminal resistance $Z$ on pressure and flow at different locations of the arterial anastomosis. From the results, it is seen that, for flow $R$ is most sensitive at nodes 1, 2 and 3, and has downstream influence, mainly on anastomosis and its parallel brachial artery. While for pressure $R$ is most sensitive locally at nodes 1, 2, and 3 with strong downstream effect on radial, ulnar and anastomosis.

anastomosis and its counterpart brachial artery (see figure 10, $E_5$). For pressure, $R$ is sensitive at nodes 1, 2 and 3 with strong downstream influence on all following nodes and upstream effects from terminal nodes due to reflections (see figure 10, $E_6$).

*(d) R sensitivity of ideal case with small Z:* Physical activities lead to a reduc-

tion in terminal resistance, $Z$ (in our study, $Z_S = \frac{Z}{30}$), which increases the blood flow and decreases mean cardiovascular pressure. As a result, the cardiac output will increase. These are the temporary changes which appear only when we do some physical exercise.

Another artificial reason for low terminal resistance is the implantation of arteriovenous fistula (AVF), which is an abnormal connection between a peripheral artery and a vein. Again for flow, $R$ is sensitive locally at nodes 1, 2 and 3 and has downstream effect on the remaining brachial nodes and on the anastomosis. For pressure, $R$ is most sensitive at first three nodes and has strong downstream influence on all nodes. For flow, a variation in $R$ within the anastomosis has small upstream sensitivity on brachial artery, while for pressure there are small upstream effects on ulnar, radial and brachial arteries (see figure 10, $E_7, E_8$).

## 4.6 Sensitivities by using a norm

Finally, we compare the results obtained by sensitivity analysis with those obtained by using norms. We found that the diameter and length of vessel are most influential parameters and that the norm computed for the wall thickness and elastic modulus has identical values (see table 2 and table 3).

| | $N_0$ | $N_1$ | $N_2$ | $N_3$ | $N_4$ | $N_5$ | $N_6$ | $N_7$ | $N_8$ | $N_9$ | $N_{10}$ | $N_{11}$ | $N_{12}$ | $N_{13}$ | $N_{14}$ | $N_{15}$ |
|---|---|---|---|---|---|---|---|---|---|---|---|---|---|---|---|---|
| | $q_0$ | $q_1$ | $q_2$ | $q_3$ | $q_4$ | $q_5$ | $q_6$ | $q_7$ | $q_8$ | $q_9$ | $q_{10}$ | $q_{11}$ | $q_{12}$ | $q_{13}$ | $q_{14}$ | $q_{15}$ |
| $E$ | 0.45 | 0.44 | 0.42 | 0.36 | 0.34 | 0.27 | 0.24 | 0.36 | 0.39 | 0.19 | 0.18 | 0.18 | 0.11 | 0.24 | 0.14 | 0.12 |
| $l$ | 0.54 | 0.53 | 0.47 | 0.43 | 0.39 | 0.32 | 0.31 | 0.95 | 0.86 | 0.48 | 0.46 | 0.25 | 0.13 | 0.34 | 0.19 | 0.15 |
| $d$ | **1.96** | **1.76** | **1.75** | **1.55** | **1.43** | **1.16** | **1.06** | **1.34** | **1.19** | **0.80** | **0.78** | **0.87** | **0.45** | **0.10** | **0.63** | **0.54** |
| $h$ | 0.45 | 0.44 | 0.42 | 0.36 | 0.34 | 0.27 | 0.24 | 0.36 | 0.39 | 0.19 | 0.18 | 0.18 | 0.11 | 0.24 | 0.14 | 0.12 |

Table 2: $\pm 10\%$ change in $E$, $l$, $d$ and $h$ at node 7 of the arm artery (see figure 4, without anastomosis) and their corresponding percentage change in flow at each node. In agreement to sensitivity computations the norm is large for change in $d$.



| | $N_0$ | $N_1$ | $N_2$ | $N_3$ | $N_4$ | $N_5$ | $N_6$ | $N_7$ | $N_8$ | $N_9$ | $N_{10}$ | $N_{11}$ | $N_{12}$ | $N_{13}$ | $N_{14}$ | $N_{15}$ |
|---|---|---|---|---|---|---|---|---|---|---|---|---|---|---|---|---|
| | $p_0$ | $p_1$ | $p_2$ | $p_3$ | $p_4$ | $p_5$ | $p_6$ | $p_7$ | $p_8$ | $p_9$ | $p_{10}$ | $p_{11}$ | $p_{12}$ | $p_{13}$ | $p_{14}$ | $p_{15}$ |
| $E$ | 0* | 0.02 | 0.03 | 0.05 | 0.06 | 0.08 | 0.08 | 0.13 | 0.13 | 0.14 | 0* | 0.09 | 0* | 0.09 | 0.10 | 0* |
| $l$ | 0 | 0.03 | 0.05 | 0.06 | 0.08 | 0.09 | 0.10 | 0.32 | 0.32 | 0.37 | 0 | 0.11 | 0 | 0.11 | 0.12 | 0 |
| $d$ | **0** | **0.13** | **0.15** | **0.21** | **0.27** | **0.33** | **0.36** | **0.58** | **0.58** | **0.63** | **0** | **0.38** | **0** | **0.40** | **0.44** | **0** |
| $h$ | 0 | 0.02 | 0.03 | 0.05 | 0.06 | 0.08 | 0.08 | 0.13 | 0.13 | 0.14 | 0 | 0.09 | 0 | 0.09 | 0.10 | 0 |

Table 3: $\pm 10\%$ change in $E$, $l$, $d$ and $h$ at node 7 of the arm artery (see figure 4, without anastomosis ) and their corresponding percentage change in pressure at each node. In agreement to sensitivity computations the norm is large for change in $d$. *Change in pressure with respect to any parameter at the boundary is zero, because we use pressure as a boundary condition.

# 5 Conclusion

The methods developed in this paper, are seen as a first step towards cardiovascular system identification from cardiovascular measurements. In this work, we have applied different methods of sensitivity analysis on linear elastic Windkessel model of the arm arteries with and without anastomosis. The results indicate a strong dependence of the pressure and flow state variables onto a variation in vessel diameter. Concerning to the elastic properties and the thickness of the arterial wall, a much lower sensitivity was found.

Alternatively, changing $R$ and $L$ in brachial artery has shown local downstream and global downstream effects on flow and pressure waves respectively. The flow, C has a strong upstream global effect from radial to brachial and ulnar to brachial, which is caused by wave reflections at the terminal nodes, 10, 12 and 15.

The method allows to determine time dependent sensitivities, which are helpful in finding optimal regions in the cardiac cycle (e.g. early systole or end diastole), from where we can get more information for estimation of parameters. For example, from the results, it is evident that the flow is sensitive on $R$ in end systole and end diastole and pressure is sensitive in early systole and early diastole. Moreover, the pressure is sensitive for $C$ in end systole and end diastole, while it is sensitive for $L$ in early systole and early diastole.

Results reveal that by changing flow control parameters, $R$, has significant local influences on flow at first three nodes (1, 2 and 3) and also have downstream sensitivities on anastomosis and its counter part brachial artery. On the other hand, pressure is most sensitive at first three nodes and all following nodes of radial, ulnar and end-to-side anastomosis.

Finally, we have used the concept of norms to quantify the results and to compare the variation in state variables according to parameter changes. We found a good agreement to the results obtained by sensitivity analysis.

# 6 Future work

The methods applied, give satisfactory results if the cardiovascular parameters are independent. In the real scenarios however, they are often interdependent like e.g. the observation of a high correlation between the extension of the elastic walls and the tangential tension caused by transmural pressure. To study these type of effects in a more general way, global sensitivity analysis has to be applied, which deals with variations in many parameters at a time.

# 7 Acknowledgments

The author would like to thank Rudolf Huttary for the fruitful discussions and encouragement.

# 8 Appendix A: Direct Differential Method (DDM)

In the DDM approach, the sensitivity coefficients are derived by differentiating eqn. (12) with respect to the model parameters, $\theta$ as

$$\frac{\partial}{\partial\theta}\Big(\dot{x}_i\Big) = \frac{\partial}{\partial\theta}\Big(Ax_i + Bu\Big) = \frac{\partial f_i(x,\theta,t)}{\partial\theta}$$

applying the chain rule and Clairaut's theorem, gives

$$\begin{aligned}
\frac{\partial}{\partial t}\Big(\frac{\partial x_i}{\partial\theta}\Big) &= A'(\theta)x_i + A(\theta)\frac{\partial x_i}{\partial\theta} + B'(\theta)u \\
\frac{\partial}{\partial t}\Big(S_i\Big) &= \underbrace{A'(\theta)x_i + B'(\theta)u}_{f_\theta} + \underbrace{A(\theta)}_{\mathrm{J}}\underbrace{\frac{\partial x_i}{\partial\theta}}_{\mathrm{S}} \\
\dot{S} &= f_\theta + J \times S,
\end{aligned}$$

where $J$ is $n \times n$ Jacobian matrix, $f$ is right hand side function in eqn. (12), $f_\theta = \frac{\partial f_i}{\partial\theta}$ and $S = \frac{\partial x_i}{\partial\theta}$.

# References


[1] Quarteroni, A., Ragni, S. and Veneziani, A., Coupling between lumped and distributed models for blood flow problems. Computing and Visualization in Science. Volume 4, 111-124 (2001).

[2] Milisic, V. and Quarteroni, A., Analysis of lumped parameter models for blood flow simulations and their relation with 1D models. Mathematical Modeling and Numerical Analysis. Volume 38, 613-632 (2004).

[3] Westerhof, N., Bosman, F., De Vries, C.J. and Noordergraaf, A., Analog studies of the human systemic arterial tree. Journal of Biomechanics, Volume 2, 121-143 (1969).

[4] Noordergraaf, A., Verdouw, P.D. and Boom, H.B.K., The use of an analog computer in a circulation model. Progress in Cardiovascular Diseases. Volume 5, 419-439 (1963).

[5] Christopher D. Prevel, MD, Hani S. et. al., The extrinsic blood supply of the ulnar nerve at the elbow: An anatomic study. The Journal of Hand Surgery. Volume 18A, 433-438 (1993).

[6] Phillips, C., A simple lumped parameter model of the cardiovascular system. PhD thesis, Colorado State University Fort Collins, Colorado (2011).

[7] Shim, E. B., Sah, J. Y. and Youn, C. H., Mathematical modeling of cardiovascular system dynamics using a lumped parameter method. Japanese Journal of Physiology. Volume 54, 545-553 (2004).

[8] Yobing, S., Lumped parameter modeling of cardiovascular system dynamics under different healthy and diseased conditions. PhD thesis, University of Sheffield (2013).

[9] Sherwin, S. J., Franke, V., Peiro, V., and Parker, K., One dimensional modeling of a vascular network in space time variables. Kluwer Academic Publishers. Volume 47, 217-250 (2003).

[10] Kappel, F. and Batzel, J., Sensitivity analysis of a model of the cardiovascular system. IEEE, Engineering and Medicine and Biology Society (conference proceedings), Aug. 30-Sept. 3. 359-362 (2006).

[11] Samira, J. et. al., Parameter sensitivity analysis of a lumped-parameter model of a chain of lymphangions in series. American Journal of Physioligy, Heart and Circulatory Physiology. DOI: 10.1152/ajpheart.00403.2013 (2013).

[12] Ataee, P. et. al., Identification of cardiovascular baroreflex for probing homeostatic stability. Computing in Cardiology (conference proceedings), Sept. 26-19, 141-144 (2010).

[13] Sumner, T., Sensitivity analysis in system biology modeling and its application to a multi-scale model of the blood glucose homeostatis. PhD thesis, University College London, UK (2010).

[14] Sato, T., Yamashiro, S.M., Vega, D. and Grodins, F.S., Parameter sensitivity analysis of a network model of systemic circulatory mechanics. Annals of Biomedical Engineering. Volume 2, 289-306 (1974).

[15] Yu, Y.C., Boston, J.R., Simaan, M.A. and Antaki, J.F., Sensitivity analysis of cardiovascular models for minimally invasive estimation of systemic vascular parameters. Proceedings of American Control Conference, San Diago, California. Volume 5, 3392-3396 (1999).

[16] Harvey, W., Exercitatio anatomica de motu cordis et sanguinis in animalibus, Frankford, chapter 14 (1628).

[17] Weber, EH., De pulsu, resorptione, auditu et tactu. Annotationes Anatomicae et Physiologicae, Lipsiae, (1834).

[18] Liebau, G., Die Bedeutung der Trägheitskräfte für die Dynamik des Blutkreislaufs. Zs Kreislaufforschung. Volume 4, 428-438 (1957).

[19] Maximilian, M., Johnnie, W. H., Graham, S. S., Thomas, K., Noordergraaf, A.,Impedance defined flow: Generalization of William Harvey's concept of the circulation-370 year later. International Journal of Cardiovascular Medicine and science, Volume 1, 205-2011 (1998).

[20] Laguy, C.A.D., Bosboom, E.M.H., Belloum, A.S.Z., Hoeks, A.P.G. and van de Vosse, F.N., Global sensitivity analysis of a wave propagation model for arm arteries. Medical Engineering and Physics. Volume 33, 1008-1016 (2011).

[21] Jager, Gerad S., Westerhof, N., Noordergraf, A., Oscillatory flow impedance in electrical analog of arterial system: representation of sleeve effect and nonnewtonian properties of blood. Circulation research. Volume XVI, 121-133 (1965).

[22] Bernhard, S., Al Zoukra, K. and Schütte, C., Statistical parameter estimation and signal classification in cardiovascular diagnosis. Environmental Health and Biomedicine. Volume 15, 458-469 (2011).

[23] Zi, Z., Sensitivity analysis approaches applied to systems biology models. IET system biology. Volume 5, issue 6, 336-346 (2011).

[24] Hindmarsh, A.C., Brown, P.N., Grant, K.E. et al. SUNDIALS: suite of nonlinear and differential/algebraic equation solvers, ACM Transactions on Mathematical Software. Volume 31, 363-396 (2005).

[25] Serban, R., Hindmarsh, A.C., CVODES: the sensitivity-enabled ODE solver in SUNDIALS. Proceedings of IDETC/CIE (2005).